

## THERMAL PERFORMANCE OF THE THERMAL STORAGE ENERGY WITH PHASE CHANGE MATERIAL

Paweł BAŁON<sup>\*</sup>, Bartłomiej KIEŁBASA<sup>\*</sup>, Łukasz KOWALSKI<sup>\*</sup>, Robert SMUSZ<sup>\*\*</sup>

<sup>\*</sup>AGH University of Science and Technology, Faculty of Mechanical Engineering and Robotics,  
 al. Mickiewicza 30-B2, 30-059 Kraków, Poland

<sup>\*\*</sup>Rzeszów University of Technology, ZT, Aleja Powstańców Warszawy 12, 35-959 Rzeszów, Poland

[balonpawel@gmail.com](mailto:balonpawel@gmail.com), [bartek.kielbasa@gmail.com](mailto:bartek.kielbasa@gmail.com), [lkowalski@agh.edu.pl](mailto:lkowalski@agh.edu.pl), [robsmusz@prz.edu.pl](mailto:robsmusz@prz.edu.pl)

*received 11 September 2022, revised 18 November 2022, accepted 2 December 2022*

**Abstract:** Values of energy supply and demand vary within the same timeframe and are not equal. Consequently, to minimise the amount of energy wasted, there is a need to use various types of energy storing systems. Recently, one can observe a trend in which phase change materials (PCM) have gained popularity as materials that can store an excess of heat energy. In this research, the authors analysed paraffin wax (cheese wax)'s capability as a PCM energy storing material for a low temperature energy-storage device. Due to the relatively low thermal conductivity of wax, the authors also analysed open-cell ceramic Al<sub>2</sub>O<sub>3</sub>/SiC composite foams' (in which the PCM was dispersed) influence on heat exchange process. Thermal analysis on paraffin wax was performed, determining its specific heat in liquid and solid state, latent heat (LH) of melting, melting temperature and thermal conductivity. Thermal tests were also performed on thermal energy container (with built-in PCM and ceramic foams) for transient heat transfer. Heat transfer coefficient and value of accumulated energy amount were determined.

**Key words:** energy storage, phase change material, PCM, heat accumulation

### 1. INTRODUCTION

Energy accumulation plays an important role in sustainable utilisation of available energy sources and in improving their efficiency [1]. It happens due to some energy sources being available for limited timeframes, such as solar energy and waste heat emitted by machines, home appliances and buildings [1]. Phase change materials (PCM) provide the opportunity to accumulate such heat energy because of their relatively large values of latent heat (LH). Energy accumulation systems utilising PCM are characterised by ability to store or release large amounts of energy, maintaining almost constant temperature value when the phase transition occurs. They are used in multiple fields: solar energy (solar water heating, solar air heating [2, 3, 4], solar power plants [4]), construction of passive and active energy-storage systems [5], photovoltaic panel cooling [6], electronics [7], automotive industry [8], space heating and domestic hot water systems [9], space cooling systems [10], spacecraft industry, food industry, for biomedical appliances and intelligent textiles. The first studies in the literature dealing with PCM are dated back to the '40s of the preceding century [11], but only the energy crisis during the '70s led to their utilisation as thermal energy storages (TES) that can release sensitive heat (SH) or LH, and visibly increased PCMs' importance for energy management [12, 13]. PCMs can be grouped based on their origin as organic, non-organic or eutectic mixtures. Organic PCMs can be further divided into paraffins, fatty acids and ionic liquids. Inorganic PCMs are mostly salts, their hydrates and eutectic mixtures created with them. They are typically characterised by high values of enthalpy of fusion, a small

range of phase transition temperature and higher – in comparison with organic PCMs – thermal conductivity coefficients. However, inorganics are not thermally stable during phase transition – they undergo segregation and might be supercooled. Such occurrences can cause corrosion of PCM containers. Organic PCMs have a relatively high value of LH, are chemically stable and their melting temperature can be controlled by regulation of carbon atoms' amount in chain during the synthesis process. The disadvantages of using organic PCMs include their tendency to change volume during melting, as well as low thermal conductivity coefficients. For example, salt's hydrates have thermal conductivity coefficients within the range of 0.4–0.7 W/(mK) [14] while organics have it in the range of 0.15–0.3 W/(mK) [15]. Organics don't cause corrosion, are non-toxic and the supercooling effect during phase change is relatively small in their case. Organic PCMs are readily available in relatively low prices, characterised by a wide range of work temperatures to choose from, chemically stable and safe to use with drinking water and various other materials [16]. Given the small thermal conductivity coefficients of the materials discussed above, the issue of intensifying heat transfer presents a scientific problem. One of its solutions is to disperse the material in another body, which is able to transfer the heat well (such as metals and their alloys). The conducting material can be structured as a frame, net, porous foam etc., with copper and aluminium foams or expanded graphite allowing mention as examples. Porous ceramic materials can also be used. Additionally, PCM containers can be equipped with parts that intensify the heat exchange process, such as ribbed structures [17, 18, 19, 20], metal meshes and rings. Another way to intensify the heat exchange rate is the utilisation of nanomaterials mixed with PCMs to increase the

thermal conductivity coefficient of such blends in comparison with the raw material [21, 22, 23]. The container shape plays a major role in the heat exchange process as well, e.g. a container shaped as a cylindrical ring displays better thermal characteristics than a spherical one of the same volume.

In this research, the authors used ceramic open-cell composite foams of Al<sub>2</sub>O<sub>3</sub>/SiC. The advantage of using such foams is their low weight in comparison with metallic foams, as well as a lower price. It has to be noted that, unfortunately, the heat transfer coefficient for ceramic foams is lower than that for foams based e.g. on aluminium alloy or copper.

Pure Al<sub>2</sub>O<sub>3</sub> has a thermal conductivity coefficient of 18 W/mK [24], which can be increased by adding SiC to the material up to 35 W/mK, with a 43% SiC weight admixture [25].

Utilisation of a ceramic array should perceptibly increase the heat exchange rate during the charging process of a container with PCM. It should lower the time required to charge and discharge the heat energy from and into the PCM heat accumulation system.

## 2. THERMAL PROPERTIES OF THE PCM

In this research, paraffin (cheese) wax was used as PCM, and it is composed of refined petroleum slack and beeswax. Paraffins are materials consisting of saturated carbon–hydrogen chains (with C<sub>n</sub>H<sub>2n+2</sub> formula) integrated with branched, straight and ring-like (aromatics) structures, which are produced by the distillation of crude oil. Both the melting point temperature and LH of fusion increase with chain length. For an n in between 5 and 17, they are liquid at room temperature, while those with an n higher than 17 manifest in the form of solids. With an increasing number of carbon atoms, the melting temperature of paraffin waxes is also increased. Solid paraffin waxes are a mixture of hydrocarbons (iso-alkanes and cycloalkanes). For this reason, it is also difficult to accurately determine the molar mass of paraffins. Cheese wax is considered non-toxic, which is important for PCM TES that are intended for application in drinking water preparation. This type of paraffin (cheese wax) is used to protect cheese. No legal restrictions apply and they can be used as a PCM in domestic hot water tanks, without additional tests and approvals. And this is very important from a practical point of view.

Concerning the present study, the first measurements performed were those of specific heat, LH and phase transition temperature. Specific heat measurements of the discussed PCM were performed using a differential scanning calorimeter (DSC) Mettler-Toledo DSC 822e with IntraCooler Haake EK 90/MT under a nitrogen atmosphere (60 ml/min flow speed) [Fig. 1]. The test was performed using standard DSC aluminium crucibles with a 40 μl volume. Temperature appreciation speed was set to 10 °C/min. Specific heat measurements were performed in accordance with recommendations in the literature [26, 27].

Specific heat measurement was performed using an indirect method with a sapphire calibration constant temperature growth rate of 10 °C/min and heat flux (HF) being the directly measured value [28].

Samples of a weight between 5 mg and 20 mg were taken from provided material (Fig. 2).

In the first experimental step, the heat rate with an empty container ( $HF_{cr}^{exp}$ ) was recorded. After placing the sample in the crucible, the measurement was repeated, obtaining HF readings

of samples with crucibles  $HF_{pr+cr}^{exp}$ . HF for the sample follows the formula:

$$HF_{pr}^{exp} = HF_{pr+cr}^{exp} - HF_{cr}^{exp} \quad (1)$$

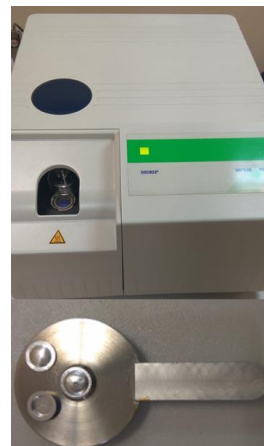


Fig. 1. DSC DSC822e and crucibles used. DSC, differential scanning calorimeter

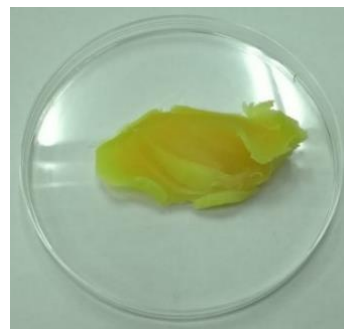


Fig. 2. Plastic wax analysed in the research

In the next step, heat rate on the reference material (sapphire)  $HF_{sap}^{exp}$  was measured. The reference material was a sapphire disc with a diameter of 7 mm, which was directly analysed in the calorimeter's chamber.  $HF_{sap}^{exp}$  was obtained by subtracting the HF signal for sapphire from the signal measured with the device's chamber when it was empty. It allowed determination of the specific heat of the reference sample, following the formula:

$$c_{psap}^{exp} = \frac{HF_{sap}^{exp}}{m_{sap} \beta} \quad (2)$$

where  $HF_{sap}^{exp}$  represents the heat rate with the reference sample (mW),  $m_{sap}$  the reference sample's weight (mg) and  $\beta$  the rate of temperature change during the test (K/min).

Afterwards, the correction factor K, used to account for heat loss to the environment, was calculated:

$$K = \frac{c_{psap}^{lit}}{c_{psap}^{exp}} \quad (3)$$

where  $c_{psap}^{lit}$  represents the standardised specific heat of a sapphire reference (J/[gK]) [28].

The experimental value of the specific heat of the samples was determined using Eq. (1) and in compliance with the following relationship:

$$c_{p_{pr}}^{exp} = \frac{HF_{pr}^{exp}}{m_{pr} \beta}, \quad (4)$$

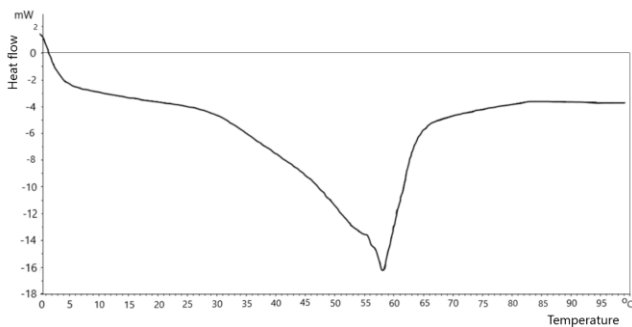
where:  $m_{pr}$  represents the sample weight (mg), and  $\beta$  the rate of temperature change during the test (K/min).

Weights of wax samples and the sapphire reference sample were measured using an analytical balance. The specific heat of PCM samples was calculated using the following relationship:

$$c_{p_{pr}}^{cor} = c_{p_{pr}}^{exp} K, \quad (5)$$

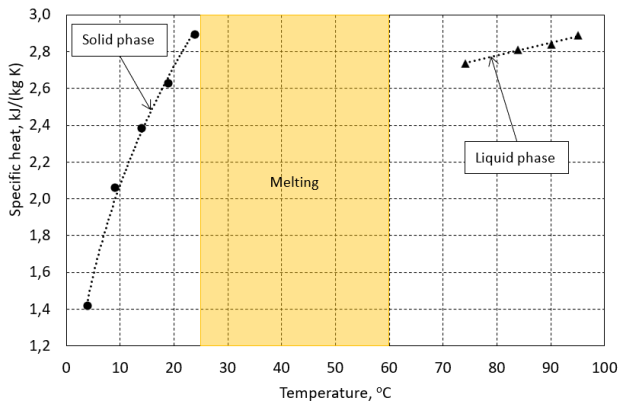
where:  $c_{p_{pr}}^{cor}$  represents the sample's specific heat after correction (J/[gK]).

Fig. 3 presents the DSC thermograph of a HF signal measured for the wax sample after subtracting the signal measured with the empty crucible.



**Fig. 3.** Wax DSC thermogram – identification of specific heat. DSC, differential scanning calorimeter

Values of the specific heat of PCM specimens calculated using the procedure described above are presented in Fig. 4 (for solid and liquid states of the material).



**Fig. 4.** Specific heat of wax vs. temperature

For the solid phase, a major increase of heat capacity is perceptible in the dependence of temperature, achieving the value of 2.9 kJ/(kgK) in 25 °C. A relatively small increase of specific heat can be observed for the material in its liquid state.

**Tab. 1.** Specific heat capacity of the paraffin wax [29]

Melting temperature (°C)	Specific heat capacity (kJ/kgK)	
	Solid	Liquid
32–32.1	1.92	3.26

The measured average specific heat for the solid phase amounts to 2.3 kJ/kgK and is slightly higher than the data presented in the literature [29].

In turn, for the liquid phase, the measured average specific heat is 2.99 kJ/kgK, which is less than the value presented in the literature [29]. The discrepancies are probably due to the different carbon–hydrogen chains' structure of the paraffin in the solid state and the fact that the tested sample is composed of refined petroleum slack and beeswax. This is also evidenced by the higher melting point, as shown in Tab. 1.

The LH of melting and melting temperature for the analysed material were determined using DSC analysis in compliance with the standards presented in the literature [30, 31, 32], with indium being used as a reference material for determination of the LH of melting.

$$L = L_c \frac{m_c A}{m A_c} \quad (6)$$

where:  $L$  represents the LH of melting for the sample,  $L_c$  the LH of melting for the reference material,  $m$  the specimen weight,  $m_c$  the reference weight,  $A$  the surface area under the HF graph (as marked in Fig. 5) for the sample and  $A_c$  the area on the HF graph for the reference material.

A temperature range for this measurement was selected based on the sample's material characteristics. Tests were carried out through the aid of the same calorimeter as for previous trials (Mettler-Toledo DSC822e, in nitrogen with its flow speed equal to 60 ml/min), using an IntraCooler device.

As visible in Fig. 5, DSC analysis of the wax sample showed a single-step melting process with very small differences between the heating cycles. For each of the tests, there is one peak in the melting process. The peak on each DSC curve represents a phase change. As can be seen in Fig. 5, due to the presence of multicomponent hydrocarbon isomers, paraffin does not have a clear (sharp) melting temperature. The melting process of wax does not occur in a constant temperature, but rather in a range of temperature values, which starts at 25 °C and ends at 60 °C. In the initial part of the transition, the LH is relatively small, while soaring LH values can be observed at 53 °C, which corresponds to the calculated melting temperature of the tested PCM.

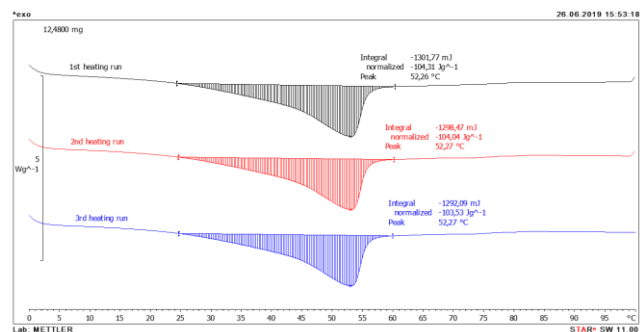


**Fig. 5.** Wax DSC thermograms – identification of the latent and melting temperatures. DSC, differential scanning calorimeter

To determine the LH of melting of PCM, three tests were performed, and their results are presented in Tab. 2. Small differences in the calculated LH lead to the conclusion that the phase-change and thermal properties of the material are stable, making it suitable for use in TES systems.

Tab. 3 shows the properties of the paraffins. Compared to the values measured in this study, the melting enthalpy of paraffins is more than twice as high. This is because, as mentioned before, paraffins consist of carbon–hydrogen chains and this may indicate shorter chains for the tested sample. Therefore, the LH of the cheese wax is much lower.

Tab. 2. Results of measuring the melting point and LH of the paraffin wax

Test No.	Melting temperature (°C)	LH (kJ/kg)
1	52.3	104.31
2	52.3	104.04
3	52.3	103.53
<b>Mean</b>	<b>52.3</b>	<b>104.0</b>

LH, latent heat

Tab. 3. The thermal properties of paraffins

Paraffin	No. of carbon atoms in one molecule	Melting temp. (°C)	LH (kJ/kg)	Density (kg/m <sup>3</sup> )
n-Nonadecane	19	32	222	785
n-Eicozane	20	36.6	247	788
n-Heneicozane	21	40.2	213	791
n-Docozane	22	44	249	794
n-Trikozane	23	47.5	234	796
n-Tetracozane	24	50.6	255	799
n-Pentacozane	25	53.5	238	801
n-Hexacozane	26	56.3	256	803
n-Heptacozane	27	58.8	235	779
n-Oktacozane	28	41.2	254	806
n-Nonacozane	29	63.4	239	808
n-Triacontane	30	65.4	252	775

LH, latent heat

Uncertainty in measurement of specific heat and LH was estimated using the procedures described in the literature [33, 34]. Complex standard uncertainty was calculated according to the formula:

$$u_c(Y) = \sqrt{\sum_{j=1}^n \left( \frac{\partial Y}{\partial X_j} u(X_j) \right)^2} \quad (7)$$

where:  $u(X_i)$  represents standard uncertainties of partial measurements and  $u_c(Y)$  total complex standard uncertainty.

The following factors influence the uncertainty in determination of the specific heat and the LH of fusion: repeatability of heat power measurements for an empty cell, empty crucibles, sample and sapphire, and determination of the mass of the sample, sapphire and indium. The uncertainty in the heat power measurement is  $\pm 0.1$  mW. The error of mass measurement with the analytical balance was determined at the level of  $\pm 0.01$  mg. The uncertainty in the specific heat and the LH of fusion for the thermal power was estimated at the level of  $\pm 3\%$ . In the next step, measurements of PCM's thermal conductivity coefficient were carried out using a KD2 thermal properties analyser (Decagon Devices Inc.) This device can be used to measure properties of solid, loose and liquid materials [35]. The method of calculating the thermal conductivity coefficient is based on solving temperature functions:

– For heating phase:

$$T(t) = m_0 + m_2 t + m_3 \ln(t) \text{ for } 0 < t \leq t_h, \quad (8)$$

– For cooling phase:

$$T(t) = m_1 + m_2 t + m_3 \ln\left(\frac{t}{t-t_h}\right) \text{ for } t > t_h, \quad (9)$$

$$k = \frac{q}{4\pi m_3} \quad (10)$$

where:  $T(t)$  represents the temperature of a linear heat source,  $m_0, m_1, m_2$  and  $m_3$  indicate constants,  $m_0$  should be interpreted as the environment temperature during the heating phase considering contact resistance,  $m_2$  the velocity of environment temperature drift,  $m_3$  the slope of temperature function vs.  $\ln(t)$ ,  $k$  the thermal conductivity coefficient,  $q$  the power of this linear heat source and  $t_h$  the operating time of the linear heat source.

By registering temperature change over time and approximating the collected data with Eqs (8) and (9), it is possible to determine the thermal conductivity coefficient value. To measure the thermal conductivity of PCM in the liquid and solid states, a KS-1 measurement probe (length 60 mm and diameter 1.3 mm) was used. The probe enables measurement of the thermal conductivity coefficient of solids and liquids in the range of 0.02–2.00 W/(mK) within a temperature range of  $-50$  °C to 150 °C, with a  $\pm 5\%$  accuracy in the range 0.2–2.0 W/(mK), and  $\pm 0.01\%$  in the range 0.02–0.2 W/(mK) [36].

The analysed wax samples in glass vials were placed in a water bath, controlling the water temperature, as indicated in Fig. 6. After reaching thermal equilibrium of the system, four measurements were performed for each analysed temperature value. The results of the experiment are indicated in Fig. 7. The solid phase measurements exhibited a strong temperature dependency, where thermal conductivity peaked at 35 °C, possibly due to the solid–solid structural transition [37].

One can observe that the thermal conductivity almost doubled during the melting process, in comparison with the commencement of the experiment, at which time this value was recorded at 25 °C. It was seen during melting that the sample was highly viscous with a mush-like characteristic. It was observed that for paraffins with a higher melting temperature, there occur both structural and state changes [37, 38], similar to this case. In general, for paraffins with a higher melting point, there may be another “phase”, consisting of solid flakes (particles) and liquid cells, which is called the mush phase. During structural change, a single phase undergoes thermal excitation, which results in the conversion (rebuilding) of the internal structures of the paraffin, and this is known as the solid–solid phase change.

The structure of the carbon–hydrogen chains changes and might have affected how energy is transferred between solid particles of the paraffin wax (molecular mechanism of heat conduction in a solid) [39].

Therefore, a strong increase in the heat conductivity coefficient during melting is the result of the reconstruction of the paraffin structure. This phenomenon is correlated with the structural change. After finalising the structural transition, thermal conductivity decreases to its minimal value for liquid wax, and then slowly increases with temperature. With the appearance of cells containing a liquid phase, convective heat exchange processes begin to dominate. This causes a strong decrease in the thermal conductivity of the paraffin wax. The particular values of this phenomenon are presented in Tab. 4.



**Tab. 4.** Thermal conductivity of the paraffin wax

Melting temperature (°C)	Thermal conductivity (kJ/kgK)		Reference
	Solid	Liquid	
32–32.1	0.514	0.224	Francis Agyenim
51.8	0.233	n/a	Mohamed Lachheb
53–57	0.26	0.16	Vahit Saydam

The measured values of the thermal conductivity coefficient for the solid phase that find mention in the literature [40, 41] are observed to be much higher than the values reported in the present study. The probable cause of these higher values might be the fact of the measurement having been made already, at the beginning of the phase transition. As can be seen from Fig. 7, there is a rapid increase in the thermal conductivity coefficient between the temperatures of 25.2 °C and 25.6 °C.

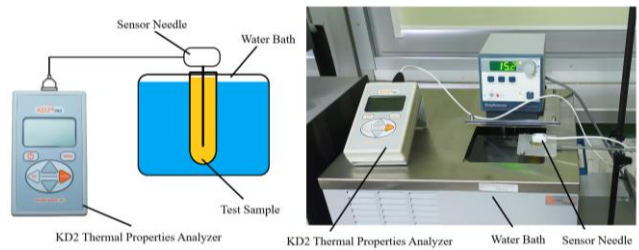


**Fig. 6.** Schematic diagram of thermal conductivity test equipment

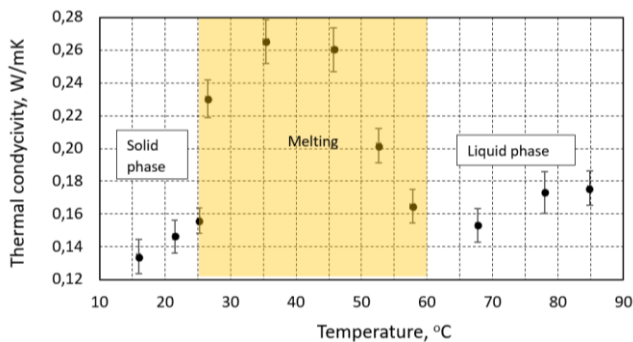


**Fig. 7.** Thermal conductivity of the wax vs. temperature

Standard uncertainty was calculated in accordance with recommendations in the literature, and its values are presented in Tab. 5.

**Tab. 5.** The melting point and the LH of the wax

Temperature (°C)	Standard uncertainty in the temperature (°C)	Thermal conductivity (W/[mK])	Standard uncertainty in the thermal conductivity (W/[mK])
16.0	0.30	0.134	0.010
21.5	0.26	0.146	0.010
25.2	0.27	0.156	0.008
26.5	0.30	0.230	0.012
35.4	0.37	0.265	0.013
45.7	0.30	0.260	0.013
52.6	0.28	0.202	0.010

57.8	0.36	0.165	0.010
67.7	0.33	0.153	0.010
78.0	0.28	0.173	0.013
84.8	0.28	0.176	0.010

LH, latent heat

The last determined material parameter was the density of the wax in its solid state and at a temperature of 22 °C. The value was determined using an analytical scale and with manual measurement of a cylindrical specimen. The obtained density value was 909 kg/m<sup>3</sup> with an uncertainty of ±1%.

### 3. THERMAL PERFORMANCE OF THE STORAGE CONTAINER WITH PCM AND CERAMIC FOAM

In the following step, the authors researched the thermal properties of PCM dispersed in Al<sub>2</sub>O<sub>3</sub>/SiC composite foams, utilising an experimental TES system with a measurement setup designed for the purpose. Porosity of the foam was determined using optical analysis [42] with a help of open source software [43]. One of the most frequently used methods of porosity measurement is the Archimedes method, applied according to the EN 623-2 standard [44]. However, if the pore size is >200 μm, this method is not recommended for porosity measurements. In this case, the pore sizes were in the range of 1.5–3.0 mm. Therefore, the optical technique was used to measure the porosity of the Al<sub>2</sub>O<sub>3</sub>/SiC composite. This measuring technique is successfully used to determine the porosity of building materials, rocks, etc. The samples were photographed in a high resolution. Then, to further clean the image, a threshold value was set using an open-source photo editing software (ImageJ, an image processing program), so that any given pixel was either white or black (Fig. 8).

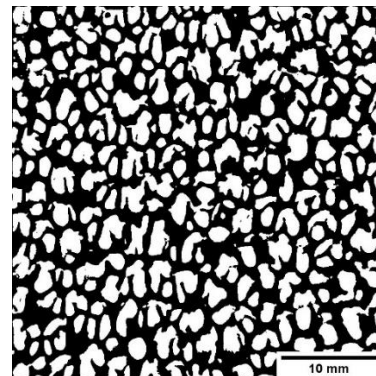


**Fig. 8.** Photographed image of ceramic foam (pores are white)

Then, the area of the pores and the skeleton was measured, and on this basis, the porosity was determined. Three samples of the foam were appraised to obtain a mean porosity of 48%. Then, the foam was placed in a cuboidal container (with a volume of 2.3 l), and filled with cheese wax afterwards (Fig. 9). The container was placed inside a case, which made it easier to mount probes and measurement devices to the rig and enable water-flow inside. During tests, the “hot” side of the rig was heated with flowing liquid (water), and the “cold” side was thermally insulated. A thin HF meter (OMEGA®, with 5% declared measurement uncer-

tainty) was fixed to the “hot” side of the PCM container, in addition to the installation of two K-type thermocouples with which to measure the container’s surface temperature. Additionally, three K-type thermocouples were installed in the space between the device’s case and the container, to measure the flowing fluid’s temperature. Five K-type thermocouples were also placed on the “cold” container’s side.

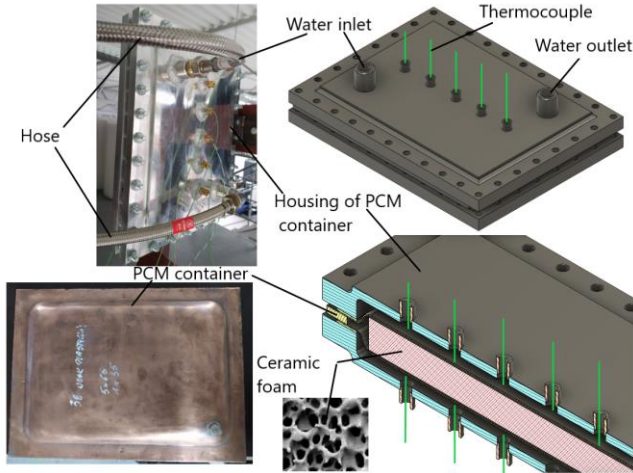


Fig. 9. View of the measuring section and the PCM container. PCM, phase change material

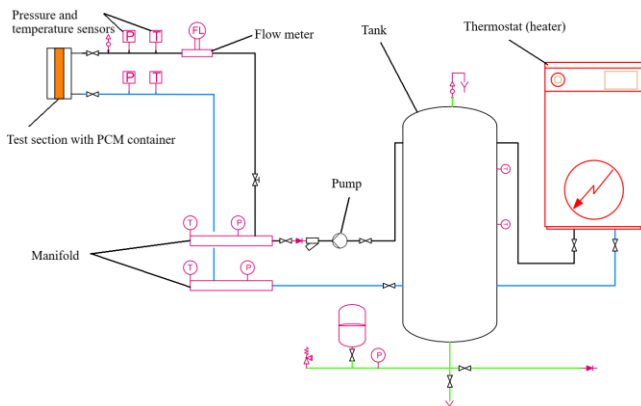


Fig. 10. Simplified scheme of the experimental stand

The test section was integrated into the experimental stand (Fig. 10). The stand consists of main parts such as: buffer tank, measurement/test section, pump and thermostat (heater). The buffer tank is included in the setup to maintain the stability and uniformity of the temperature at which hot water is supplied to the test section. The liquid’s flow rate through the measurement section was regulated using a valve, and measured with a TecFluid TM44 turbine flowmeter. The temperatures on the inlet and outlet of the test section were measured using Pt100 thermistors, while the water-pressures at these same locations were read using WIKA piezoelectric transducers. For data acquisition, a DATAQ®

Instruments GL820 midi Logger was used.

For the duration of the trials, the following parameters were logged:

- the test section’s inlet and outlet temperatures;
- the water-pressures of the inlet and outlet;
- the volumetric flow rate;
- the temperature of the PCM container’s external surfaces;
- the temperature of the surrounding environment; and
- the HF.

The data obtained were recorded in a text file. The main objective of this study was to determine the heat exchange conditions prevailing during the TES charging process and the amount of accumulated heat energy. To obtain the heat transfer coefficient, HF density on the container’s surface was measured along with the temperatures of the fluid and of the aforementioned surface, with the liquid’s volumetric flow rate being ascertained at 0.57 m<sup>3</sup>/h.

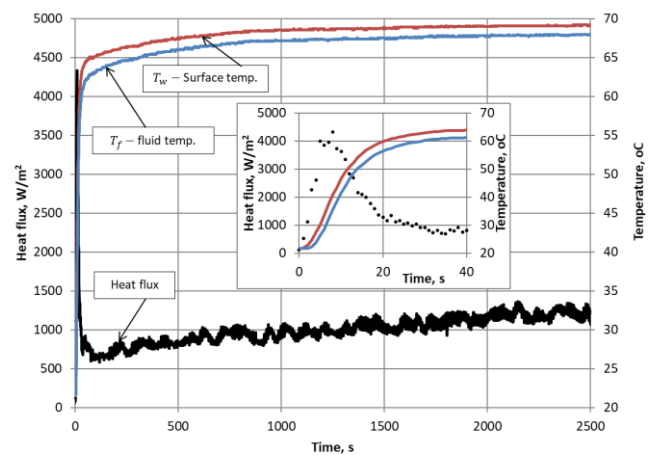


Fig. 11. HF density, fluid and surface temperature vs. time. HF, heat flux

At the beginning of the charging process, the HF from water to the PCM container grows rapidly, as shown in Fig. 11. This phenomenon is followed by a similar-in-size fast decrease and stabilisation of the parameter, with a slight increase over time. The initial growth of HF can be explained by the large difference between the temperatures of the container and the liquid at the beginning of a charging process. During forced convection, the temperature difference between the fluid and the wall is the main driving force in the process of thermal energy transport. Moreover, in the initial heat transfer process, the thickness of the thermal boundary layer is small. The thermal resistance of the boundary layer is very low and therefore the transfer coefficient attains high values. After the system’s temperature becomes regulated, the “driving force” behind this HF’s spike decreases. This is due to the stabilisation and growth in the thickness of the thermal boundary layer. The function of heat transfer coefficient in time was determined using the following formula:

$$h(t) = \frac{q(t)}{T_f(t) - T_w(t)} \quad (11)$$

where:  $h(t)$  represents the transient heat transfer coefficient,  $q(t)$  the HF,  $T_f(t)$  the temperature of the liquid and  $T_w(t)$  the container’s wall temperature.

Change of the heat transfer coefficient across time is presented in Fig. 11. Similarly as with the HF density graph, a spike of the coefficient’s value is observed at the beginning of the process. It

can be explained by the relatively small thickness of the container's wall, enabling rapid heat exchange with large temperature differences of the container and a medium. The slight increase of the coefficient's value afterwards can be caused by a decrease in the fluid's viscosity at the container's surface as it accumulates more energy, intensifying fluid transport momentum.

The mean value of heat transfer coefficient  $\bar{h}$  was calculated as a mean of the function:

$$\bar{h} = \frac{1}{t} \int_0^t \frac{q(t) dt}{T_f(t) - T_w(t)} \quad (12)$$

where:  $t$  indicates time.

The mean heat transfer coefficient calculated for a timeframe between 0 s and 2,500 s is 780 W/m<sup>2</sup> K, proving that the heat exchange process is laminar.

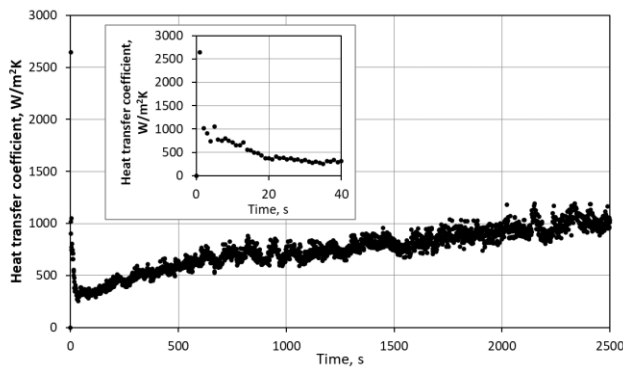


Fig. 12. Instantaneous value of the heat transfer coefficient

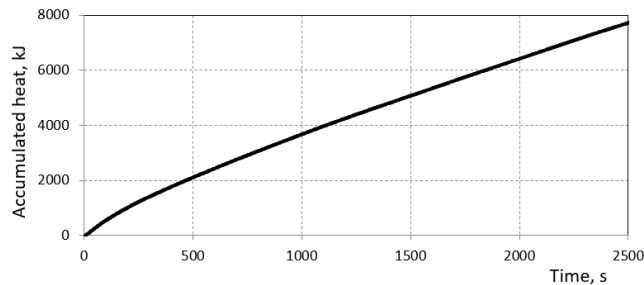


Fig. 13. The amount of accumulated heat

The amount of heat accumulated during charging process ( $Q$ ) was calculated based on the relation:

$$Q = \int_0^t \rho c \dot{V} [T_{in}(t) - T_{out}(t)] dt \quad (13)$$

where:  $\rho c$  represents the volumetric heat capacity of water,  $\dot{V}$  water's volumetric flowrate,  $T_{out}$  temperature of water in the test section's outlet and  $T_{in}$  temperature of water in the test section's inlet. Water's volumetric heat capacity, which is a product of specific heat and density, was calculated, based on literature data [44, 45], to be the following:

$$\rho c = 4211.7 - 1.6796 T_{av} \quad (14)$$

where:  $T_{av}$  temperature is an arithmetic mean of inlet's and outlet's liquid temperatures.

The determined amount of accumulated heat is presented on graph (Fig. 13). As visible, the amount of heat accumulated is an ascending linear function of time, except the beginning of the charging process. The slope of the curve presented in Fig. 13

depends on the heat capacity of the paraffin as well as on the heat transfer coefficient. The higher intensity of heat accumulation observed in the initial phase (Fig. 13) is related to higher values of the heat transfer coefficient, as shown in Fig. 12. The use of ceramic foam eliminates the effect (local change of the curve slope) related to the phase change [46, 47, 48].

#### 4. SUMMARY

In this study, the authors carried out research on the thermal properties of a PCM – specifically wax. In the dominant majority of publications focussed on PCM materials, the description of the thermophysical properties is limited to information concerning only the LH, melting point temperature and (less often) the thermal conductivity coefficient (for the solid and liquid phases). There is a noticeable absence of complete information on changes in thermophysical properties during the phase change. Therefore, in this study, detailed thermophysical studies were carried out during the wax melting process. In particular, the temperature range in which the phase change occurs was precisely determined. This is important for the correct design of thermal energy accumulation systems.

Specific heat was determined for the material's solid and liquid states. In the material's solid state, a strong increase of specific heat capacity in relation to temperature increase is observed, reaching 2.9 kJ/(kgK) at a temperature of 25 °C. In the material's liquid state, a slight and approximately linear increase of specific heat with temperature growth was observed. DSC analysis revealed a one-stage melting process of the discussed substance, with very small differences in material behaviour during multiple subsequent heating cycles. The melting process of the analysed PCM occurs gradually in a range of temperatures starting at 25 °C and concluding at 60 °C. At the beginning of a melting process, the intensity of phase change LH's emission is relatively small. Vigorous increase of this value can be observed at 53 °C, which corresponds to the melting temperature determined in this research. The melting temperature and LH of melting were also determined as 52.3 °C and 104.0 kJ/(kgK), respectively. Omittable value differences for the LH of melting between different specimens shows that the analysed material possesses stable thermal properties. This is important for design purposes connected with TES devices and systems.

The heat transfer coefficient of wax was measured. Its value perceptibly varies with temperature changes. Above the temperature of 25 °C, it starts growing rapidly, to reach a value that is almost double its initial value, due to the material's phase transition. After a liquid phase appears, the heat transfer coefficient rapidly decreases and afterwards slightly grows with further temperature increase. The thermal analysis of a transient process of charging a PCM container filled with ceramic foam and wax was carried out. The analysis revealed that the value of the heat transfer coefficient grows rapidly at the beginning of the charging process, a phenomenon possibly caused by the small thickness of the near-wall thermal layer. This layer increases its thickness with time, thereby causing an associated decrease in the coefficient's value. Slight and steady growth of the coefficient afterwards can be caused by a decrease in the liquid's viscosity in the near-wall area.


## REFERENCES

1. Tao YB, He Y-L. A review of phase change material and performance enhancement method for latent heat storage system. *Renew. Sustain. Energy Rev.* 2018; 93: 245–259.
2. Farid MM, Khudhair AM, Siddique AK Razack, Al-Hallaj S. A review on phase change energy storage: materials and applications. *Energy Conversion and Management.* 2004; 45:1597–1615.
3. Sharma A, Tyagi VV, Chen CR, Buddhi D. Review on thermal energy storage with phase change materials and applications. *Renewable and Sustainable Energy Reviews.* 2009; 13: 318–345.
4. Agyenim F, Hewitt N, Eames P, Smyth M. A review of materials, heat transfer and phase change problem formulation for latent heat thermal energy storage systems (LHTESS). *Renewable and Sustainable Energy Reviews.* 2010; 14: 615–628.
5. Kalnæs SE, Jelle BP. Phase change materials and products for building applications: A state-of-the-art review and future research opportunities. *Energy and Buildings.* 2015; 94: 150–176.
6. Chandel SS, Agarwal T. Review of current state of research on energy storage, toxicity, health, hazards and commercialization of phase changing materials. *Renewable and Sustainable Energy Reviews.* 2017; 67:581–596.
7. Ren Q, Guo P, Zhu J. Thermal management of electronic devices using pin-fin based cascade microencapsulated PCM/expanded graphite composite. *Int J Heat Mass Transf.* 2020; 149:119199.
8. Pielichowska K, Pielichowski K. Phase change materials for thermal energy storage. *Progress in Materials Science.* 2014; 65: 67–123.
9. Douvi E, Pagkalos C, Dogkas G, Koukou MK, Stathopoulos VN, Caouris Y, Vrachopoulos MG. Phase change materials in solar domestic hot water systems: A review. *International Journal of Thermofluids.* 2021; 10:100075.
10. Souayfane F, Fardoun F, Biwole P-H. Phase change materials (PCM) for cooling applications in buildings: A review. *Energy and Buildings.* 2016; 129: 396-431.
11. Nair AM, Wilson C, Huang MJ, Griffiths P, Hewitt N. Phase change materials in building integrated space heating and domestic hot water applications: A review. *Journal of Energy Storage.* 2022; 54:105227.
12. Schaeztle WJ. *Thermal energy storage in aquifers: design and applications.* 1980; New York: Pergamon.
13. Schmidt FW. *Thermal energy storage and regeneration.* 1981; New York: McGraw-Hill.
14. Naplocha K., et al. Effects of cellular metals on the performances and durability of composite heat storage systems. *Int. J. Heat Mass Transf.* 2017; 117:1214-1219.
15. Libeer W, et al. Two-phase heat and mass transfer of phase change materials in thermal management systems. *Int. J. Heat Mass Transf.* 2016; 10: 215-223.
16. Pagkalos C, et al. Evaluation of water and paraffin PCM as storage media for use in thermal energy storage applications: a numerical approach. 2020; *Int. J. Thermofluids* 1–2.
17. Telkes M, Raymond E. Storing solar heat in chemicals—a report on the Dover house. *Heat Vent.* 1949; 46(11):80–86.
18. Quenel J, Atakan B. Heat flux in latent thermal energy storage systems: the influence of fins, thermal conductivity and driving temperature difference. *Heat Mass Transfer.* 2022. <https://doi.org/10.1007/s00231-022-03220-3>
19. Yang X, Yu J, Xiao T, Hu Z, He Y-L. Design and operating evaluation of a finned shell-and-tube thermal energy storage unit filled with metal foam. *Appl. Energy.* 2020; 261:114385.
20. Acir A, Canli ME. Investigation of Fin Application Effects on Melting Time in a Latent Thermal Energy Storage System with Phase Change Material (PCM). *Applied Thermal Engineering.* 2018.
21. Aramesh M, Shabani B. Metal foams application to enhance the thermal performance of phase change materials: A review of experimental studies to understand the mechanisms. *Journal of Energy Storage.* 2022; 50:104650.
22. Tao YB, He YL. A review of phase change material and performance enhancement method for latent heat storage system. *Renewable and Sustainable Energy Reviews.* 2018; 93: 245–259.
23. Tariq SL, Ali HM, Akram MA, Janjua MM, Ahmadlouydarab M. Nanoparticles enhanced phase change materials (NePCMs)-A recent review. *Applied Thermal Engineering.* 2020; 176:115305.
24. Jianfeng WU, Yang ZHOU, Mengke SUN, Xiaohong XU, Kezhong TIAN, Jiaqi YU. Mechanical Properties and Microstructure of Al<sub>2</sub>O<sub>3</sub>/SiC Composite Ceramics for Solar Heat Absorber. *Journal of Wuhan University of Technology-Mater. Sci. Ed.*:615-623.
25. Devaiah M, Comparison of Thermal Conductivity Experimental Results of SICP/AL<sub>2</sub>O<sub>3</sub> Ceramic Matrix Composites with Mathematical Modeling. *International Journal of Applied Engineering Research.* 2018; 13(6): 3784-3788.
26. DIN 51007 General principles of differential thermal analysis.
27. ISO 11357-4 Plastics. Differential scanning calorimetry (DSC). Part 4: Determination of specific heat capacity.
28. Ditmars DA, et al. *Jour. Res. National Bureau of Standards.* 1982; 87(2):159-163.
29. Agyenim F, Hewitt N, Eames P, Smyth M. A review of materials, heat transfer and phase change problem formulation for latent heat thermal energy storage systems (LHTESS). *Renewable and Sustainable Energy Reviews.* 2010; 14: 615–628.
30. Paris J, Falardeau M, Villeneuve C. Thermal storage by latent heat: a viable option for energy conservation in buildings. *Energy Sources.* 1993; 15: 85–93.
31. ISO 11357-3 Plastics — Differential scanning calorimetry (DSC) — Part 3: Determination of temperature and enthalpy of melting and crystallization.
32. Eysel W; Breuer KH. The calorimetric calibration of differential scanning calorimetry cells. *Thermochim. Acta.* 1982; 57(3): 317-329.
33. Coleman HW, Steele WG. *Experimentation, Validation, and Uncertainty Analysis for Engineers*, third ed. John Wiley & Sons, Inc, 2009.
34. *Evaluation of measurement data — Guide to the expression of uncertainty in measurement, GUM;* 2008.
35. *KD2 Pro Thermal Properties Analyzer Operator's Manual.* Version 10. Decagon Devices. Inc.; 2011.
36. Wang J, Xie H, Xin Z., Thermal properties of paraffin based composites containing multi-walled carbon nanotubes, *Thermochimica Acta.* 2009; 488:39-42.
37. Gulfam R, Zhang P, Meng Z. Advanced thermal systems driven by paraffin-based phase change materials - A review. *Applied Energy.* 2019; 238: 582-611.
38. Gulfam R, Zhang P, Meng Z., Phase-Change Slippery Liquid-Infused Porous Surfaces with Thermo-Responsive Wetting and Shedding States. *ACS Appl. Mater. Interfaces.* 2020; 12: 34306–34316
39. Saydam V, Duan X. Dispersing Different Nanoparticles in Paraffin Wax as Enhanced Phase Change Materials – A Study on the Stability Issue. *Journal of Thermal Analysis and Calorimetry* volume. 2019; 135: 1135-1144.
40. Lachheb M, Karkri M, Albouchi F, Ben Nasrallah S, Fois M, Sobolciak P. Thermal properties measurement and heat storage analysis of paraffin/graphite composite phase change material. *Composites: Part B* 66. 2014: 518–525.
41. de Vries DA. A nonstationary method for determining thermal conductivity of soil in situ. *Soil Sci.* 1952; 73:83-9.
42. D. Martin III Bradley, J. Putman, Nigel B. Kaye: Using image analysis to measure the porosity distribution of a porous pavement, *Construction and Building Materials*, Volume 48, November 2013, pp. 210-217



43. Image Processing and Analysis in Java-ImageJ. Available from: <https://imagej.nih.gov/ij/index.html>
44. EN 623-2 Advanced technical ceramics. Monolithic ceramics. General and textural properties. Determination of density and porosity.
45. IAPWS Industrial Formulation 1997 for the Thermodynamic Properties of Water and Steam. In: International Steam Tables. Springer. Berlin, Heidelberg. 2018.
46. Sun X, Chu Y, Medina MA, Mo Y, Fan S, Liao S. Experimental investigations on the thermal behavior of phase change material (PCM) in ventilated slabs. *Applied Thermal Engineering*. 2014; Volume 148; 5:1359-1369.
47. Bałon P., Kielbasa B., Kowalski Ł., Smusz R., Case Study on the Influence of Forming Parameters on Complex Shape Part Deformation, *Advances in Science and Technology Research Journal* 2022, 16(6):204–213
48. Wilk J., Bałon P., Smusz R., Rejman E., Świątoniowski A., Kielbasa B., Szostak J., Cieślak J., Kowalski Ł., Thermal Stratification in the Storage Tank, *Procedia Manufacturing*, 2020; 47:998–1003

The research activities comprised in this study were carried out within the LIDER IX project entitled “Development of an innovative modular energy storage system using phase change materials” (No. 0004/L-9/17/NCBIR/2018), financed by the National Centre for Research and Development.

Paweł Bałon:  <https://orcid.org/0000-0003-3136-7908>

Bartłomiej Kielbasa:  <https://orcid.org/0000-0002-3116-2251>

Łukasz Kowalski:  <https://orcid.org/0000-0002-2866-9000>

Robert Smusz:  <https://orcid.org/0000-0001-7369-1162>